Understanding the role of molar mass and stirring in polymer dissolution

Pauline Valois, Emilie Verneuil, Francois Lequeux, Laurence Talini

Cite this: DOI: 10.1039/c6sm01206j

Understanding the role of molar mass and stirring in polymer dissolution

Pauline Valois,[ab] Emilie Verneuil,*[ab] Francois Lequeux[ab] and Laurence Talini[ab]

Received 25th May 2016,
Accepted 31st August 2016

DOI: 10.1039/c6sm01206j

When a dry soluble polymer is put in contact with a large quantity of solvent, it swells and forms a transient gel, and eventually, yields a dilute solution of polymers. Everyday lab experience shows that when the molar mass is large, namely tens of times larger than entanglement mass, this dissolution process is slow and difficult and may require stirring. Here, in agreement with previous results, we found that the time needed to turn a dry grain into a dilute solution is not limited by water diffusion in the glassy or semi-crystalline dry polymer, but rather by the life-time of the transient gel made of entangled chains. In addition, we shed new light on the dissolution process by demonstrating that, in contrast to theoretical predictions, the gel life-time is not governed by reptation. We show instead that swelling is simply controlled by the osmotic pressure and the gel permeability until the overlap concentration is reached within the gel. At this stage, the gel turns into a dilute solution in which polymers are dispersed by natural convection. The observed dependence of the dissolution process on the molar mass therefore originates from the molar mass dependent overlap concentration. Under stirring, or forced convection, the polymer gel disappears at a higher critical concentration that depends on the shear rate. We suggest a description of the experimental data which uses the rheological flow curves of the solutions of the considered polymer. Inversely, dissolution times of polymer powders under stirring can be inferred from classical rheological measurements of the polymer solutions at varied concentrations.

1 Introduction

Although it constitutes a crucial step in numerous processes, the dissolution of polymers is not fully understood. It is now well established that when a solid polymer grain, either glassy or semi-crystalline, is put into contact with a solvent, a gel layer forms and, as a result, two fronts are observed.[1] The gel term simply refers to a semi-dilute entangled solution, and we will use this term as well.[2] Of the two fronts observed, one front corresponds to the interface between the dry core and the gel, the other being the interface between the gel and the solvent. As solvent diffuses into the dry core and the gel, the dry/gel interface moves inward while the gel swells and is further eroded.[3] It has been widely observed that, rather unexpectedly, for large mass polymers, the process limiting the full dissolution of the polymer is not the disappearance of the dry core but that of the gel layer. This gel is therefore the one responsible for the formation of lumps during the dissolution of powders.[4] The second result commonly reported in the literature is that the diffusion coefficients associated with the two different interfaces decrease with increasing polymer molar mass.[3,5–7] The molar mass dependence is generally believed to result from the step of chains disentanglement that is necessary for the dissolution to be completed,[3,5] as first suggested by Brochard and De Gennes[8] in a theoretical model. However, some points are unclear, in particular the fact that the velocity of the gel/solvent interface decreases too slowly with molar mass for the dissolution step of the gel to be driven by reptation.[3,9] Therefore, the relaxation mechanism of the swelling polymer network remains to be determined, as well as its influence on solvent transport from the solution into the dry polymer core compared to the driving osmotic flow.

One reason for the poor understanding of polymer dissolution lies in the complex behaviours at stake. In particular, the mutual diffusion coefficient needed to describe the flux of solvent in the polymer is expected to vary with polymer concentration.[10] The resulting diffusion profiles are complex, and have in some cases been attributed to non-Fickian diffusion processes[11–13] related to glass transition effects. However, that picture has been recently challenged,[14] and it is likely that concentration-dependent diffusion coefficients are sufficient to explain solvent diffusion in both the unswollen and swollen polymer. On the experimental side, the polymer volume fraction spans several decades during dissolution process, and a single technique cannot cover that large range. Most experimental works use

[a] Laboratoire Sciences et Ingénierie de la Matière Molle, CNRS UMR7615, ESPCI Paris, PSL Research University, 10 rue Vauquelin, F-75231 Paris, France. E-mail: emilie.verneuil@espci.fr
[b] Laboratoire Sciences et Ingénierie de la Matière Molle, Université Pierre et Marie Curie, Sorbonne-Universités, 10 rue Vauquelin, Paris, France

techniques such as NMR[3,5,6,15,16] or neutron scattering,[5,14] which probe the upper polymer concentration range. In the low concentration range, dynamic light scattering measurements have been performed in order to measure cooperative diffusion coefficient,[17] but were restricted to homogeneous polymer solution. The final stages of dissolution during which gradients of concentrations in the low concentration range are involved have thus been poorly studied.

In the present paper we address the three following questions: (i) What is the relaxation mechanism of the swollen network? (ii) What is the mechanism driving the final stage of dissolution? and finally (iii) What is the effect of shear on that mechanism? We have conducted dissolution experiments on two different polymers. We consider conditions within which the final solution after dissolution is in the dilute regime and we call dissolution the process that consists in the homogenization of the polymer concentration at large scales, *i.e.* over the typical size of the vessel of solvent. First, we show that reptation is not involved in the dissolution process of the gel, and we suggest the relaxation mechanism results from the much faster process of chain contraction in their tubes. Second, we demonstrate that dissolution is complete when the polymer concentration reaches the overlap concentration ϕ^*, which accounts for the molar mass dependence of dissolution times reported in the literature. Third, we account for the effect of stirring and we establish scaling laws for the variations of the dissolution time with the relevant parameters.

Two different types of hydrosoluble polymer were used, whose properties are detailed in the materials and methods section. First, a polyelectrolyte was chosen so as to be able to tune the osmotic pressure of the solvent inside the polymer solution by changing the salt content of the solvent. This allowed to vary the incoming flux of solvent inside the polymer and through the polymer gel surrounding the polymer grain. Second, the effect of the molar mass of the polymer was assessed in conditions where the driving mechanism for solvent penetration in the polymer was kept constant. This was achieved by using a neutral polymer with varied molar mass.

2 Materials and method

In this section we describe the properties of the used polymers, together with the different experimental set-ups we have developed to study dissolution in still water and under stirring.

2.1 Polymers

Hydrophilic polymers of high molar masses were used. First, as a giant polyelectrolyte, we used a bio fermented polysaccharide of chemical formula given in Fig. 1, and with average molar mass 5×10^6 g mol^{-1} corresponding to $N = 5.10^3$ monomers and one counter-ion per monomer. Its density is 1.5×10^3 kg m^{-3}. The entanglement concentration and reptation time of this polyelectrolyte are determined experimentally from measurements of the viscosity of aqueous polymer solutions with varied mass fraction in polymer as a function of the shear rate.

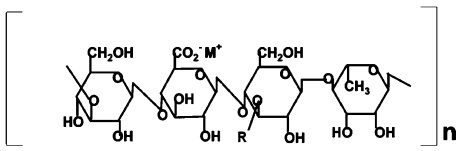

Fig. 1 Chemical formula of the polyelectrolyte used in the present work. R and M+ are proprietary information.

Typically, viscosity exhibits a plateau at low shear rate, and decreases with shear rate above a critical value. Hence, the polymer solutions exhibit a Newtonian behavior at low shear rate, and are shear thinning above the critical value. At low polymer concentration, the plateau viscosity is found to increase linearly with mass fraction, and at higher concentration, the plateau viscosity η_p increases with mass fraction ϕ as a power law with exponent 3 according to: $\eta_p(\phi) - \eta_0 = 6 \times 10^9 \phi^3$ where η_0 is the water viscosity. The entanglement concentration is determined as the crossover between the two power law regimes[18] for viscosity *versus* mass fraction, as would be done for a neutral polymer. This is of course an approximation as the polymer is a polyelectrolyte. We find: $\phi_E = 8 \times 10^{-5}$ g g^{-1}. In the entangled semi-dilute regime, from the measurement of the critical shear rate $\dot{\gamma}_A$ separating the Newtonian behavior from the shear thinning regime, the reptation time τ_{rep} is taken as the inverse of the critical shear rate.[19,20] The reptation time is found to increase with mass fraction ϕ[g g^{-1}] according to:

$$\tau_{rep} \sim \dot{\gamma}_A{}^{-1} \sim \tau_0 \phi^{1.4} \quad (1)$$

where $\tau_0 = 6 \times 10^5$ s is a characteristic time linked to the polydispersity of the polymer. Eqn (1) is in good agreement with the model by Doi and Edwards[21] for entangled solutions of polymers where reptation time is predicted to increase with mass fraction as a power-law with exponent 3/2. The use of viscosity *versus* shear rate curves to measure the reptation time is therefore validated.

By combining the measurements of the plateau viscosity *versus* mass fraction in the entangled regime ($\phi > \phi^e$) and the reptation times, the number of Kuhn segments between entanglements N_e can be calculated as $N_e = \dfrac{k_B T \tau_{rep}}{b^3\left(\eta_p - \eta_0\right)}(\phi \sim 1)$ where k_B is the Boltzmann constant, T is the temperature and $b = 3$ nm is the Kuhn length. We find $N_e = 11$.

Second, a series of polyethylene oxide polymers (PEO) was used as neutral polymers with four different molar masses M_w: 0.3×10^6 g mol^{-1}, 0.6×10^6 g mol^{-1}, 1×10^6 g mol^{-1}, and 8×10^6 g mol^{-1}. The overlap concentration of the PEO was calculated from the molar mass using results from the literature[22] where the radius of gyration of the polymer chains was measured by light scattering experiments ($R_g = 0.215 M_w{}^{0.583}$ with R_g in angstroms and M_w in g mol^{-1}) and using a theoretical relationship linking the overlap concentration to the radius of gyration taken from the literature:[10] $\phi^* = 3M_w/(4\pi 0.72^3 N_a R_g{}^3)$ where N_a is the Avogadro number. As a neutral polymer in good solvent, the entanglement concentration of PEO can be estimated from the literature[10] as $\phi_E = 7\phi^*$.

For PEO with molar masses $M_w = 1 \times 10^6$ and 8×10^6 g mol^{-1}, reptation times in aqueous solution were measured by rheology: storage and loss modulii were obtained from shear oscillatory experiments as a function of frequency. Reptation time is taken as the inverse of the frequency for which loss and storage modulii are equal to one another. For PEO with $M_w = 8 \times 10^6$ g mol^{-1} at a concentration $\phi = 0.02$ g g^{-1}, we measure $\tau_{rep} = 8$ s. Using the theoretical dependence[10] of reptation time with both polymer concentration ϕ and molar mass M_w, we obtain the semi-empirical relationship valid for $\phi > \phi_E$: $\tau_{rep}(s) \sim 9 \times 10^{-21} M_w^{3.4} \phi^{1.5}$ with M_w in g mol^{-1} and ϕ in g g^{-1}.

2.2 Preparation of thin polymer layers with controlled thickness

Polymer layers of controlled thickness were prepared from aqueous solutions at a polymer concentration of 3 wt% prepared by stirring for 24 h. A small amount (10^{-3} wt%) of sodium azide was added to prevent bacterial contamination. The polymer solutions were poured onto a glass slide within a PDMS mold of dimensions $7 \times 10 \times 20$ mm^3. After several days under ambient atmosphere, complete drying was achieved and the PDMS mold was peeled off the glass slide. We obtained dry polymer layers of inner dimensions 10×20 mm^2 and thickness $h_0 = 50 \pm 10$ μm. In equilibrium with the ambient atmosphere, these layers retain a small amount of water at a concentration ϕ_0 that was measured by thermal gravimetric analysis. The layer roughness was measured by AFM to be sub-micrometric. These polymer layers were used as such, or were used to cut out grains of given size whose swelling kinetics was measured by monitoring grains individually in a preliminary experiment.

2.3 Preliminary experiments

Polymers grains squeezed between two glass slides were put in contact with deionized water as the solvent. Observations were made with a microscope in a transmitted light mode. The initial time is taken when the grain was put in contact with water, and images of the grain were recorded over time with a CCD camera at constant exposure time and illumination intensity. A typical series of images is shown in Fig. 2.

2.4 Light scattering experiment

A home-made light scattering experiment was designed to precisely measure the swelling and dissolution kinetics of a polymer layer in pure water or brine (see Fig. 3). The polymer layers supported on glass substrates are placed at the bottom of a chamber of dimensions $150 \times 100 \times 50$ mm^3. A laser sheet of wavelength 514 nm was placed above the chamber, perpendicular to the substrate, and aligned along the longer dimension of the layer. Light scattered at a 90 degrees angle by the polymer solution was collected with a CCD camera. At initial time, water (or brine) was added to the chamber so as to fill it, and the scattered intensity was recorded during the course of the dissolution experiment along the vertical axis z at a frame rate of 0.04 Hz. The accessible concentration range was increased by shooting a series of three images with three different exposure times for every experimental times. The scattered intensity was calibrated for each exposure time of the camera against polymer

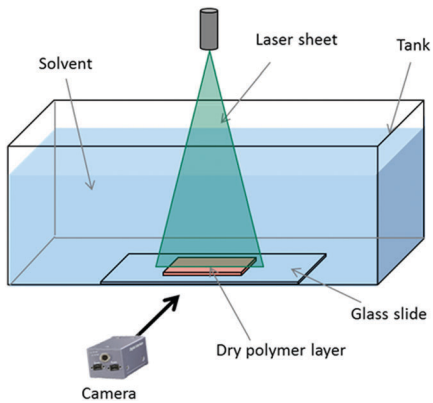

Fig. 3 Schematic representation of the experimental set-up for the measurement of the quasi-two dimensional swelling kinetics of a thin polymer layer (thickness around 50 μm) immersed into a water or brine bath. The concentration is assessed, after calibration, from the light scattered at a 90 degree angle from a laser sheet and collected by a CCD camera. The polymer concentration ϕ along the distance z to the polymer layer was obtained over time t.

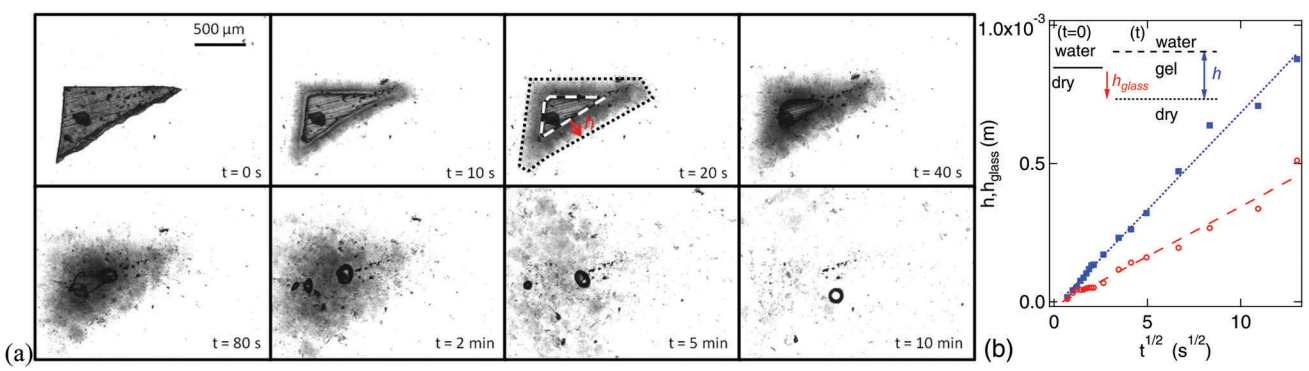

Fig. 2 (a) Time series of images of a dry polymer layer of thickness 50 μm squeezed between two glass slides and put in contact with water at initial time. Dashed line outlines the gel/dry polymer interface; dotted line delineates the gel/solution interface at an arbitrary concentration of polymer in the gel (or a given light intensity in the image). The gel thickness h is measured as the distance between the two interfaces. The dry core disappears within a minute while the gel is still visible after 10 minutes. (b) Thickness of the gel layer h and distance of the glassy/gel interface relative to the dry grain surface h_{glass} as a function of the square root of time. Lines: fits to a line with slope equal to $\sqrt{D}$ at gel/solution $D = 5.10^{-9}$ m^2 s^{-1} and glass/gel interface: $D_{glass} = 1.10^{-9}$ m^2 s^{-1}.

solutions with controlled concentration. The experimental concentration range spans between 9×10^{-5} and 1.5×10^{-2} g g^{-1}. Concentration profiles were measured over a distance of 5 mm from the polymer layer.

2.5 Microfluidic experiment

We have used the now classical silicone-based microfluidic technique to obtain a silicone cavity of height h = 50 μm, width 6 mm, and length L = 15 mm. Two injection holes were punched in the silicone chip and used as inlet and outlet for the water flow. Besides, a dry polymer layer is prepared on a glass cover slip (see Section 2.2). The height and width of the polymer layer are respectively h_0 = 50 μm and 5 mm. The polymer-coated glass slide was used as a lid for the silicone cavity: both surfaces were activated with an oxygen plasma treatment, the cavity and the polymer layer were aligned and sealed against each other. We obtained a microfluidic channel with respective height and width h_0 = 50 μm and w = 1 mm (Fig. 4). One of the channel's wall is the polymer layer. The incoming water flow rate is set by a syringe pump and the water mean velocity V in the channel ranges between 0.06 and 3 m s^{-1}. Hollow glass spheres with a diameter of 10 μm were added to the water at a very low volume fraction and used as flow tracers to confirm the value of the mean velocity of the water flow deduced from the imposed flow rate and channel geometry. The aspect ratio w/h_0 of the channel is equal to 20 and is therefore such that velocity gradients across the flow direction (in the x and z directions) develop over a distance set by the height h_0 of the channel.

The microfluidic chip was set on the stage of an inverted microscope equipped with a camera. An erosion experiment consists in filling the channel with deionized water at time t = 0 at a given flow rate and monitoring the polymer/solvent interface at mid-distance $y = L/2$ from the water inlet (Fig. 4a) and at a frame rate of 1 Hz.

2.6 Macro stirring experiment

The effect of stirring on dissolution time of a polymer powder was assessed on a homemade device. Experiments were conducted in a vessel of 6 milliliters mounted on a rheometer. The dissolution process was ensured by a stirring bar of controlled geometry spun at a controlled rotation speed. The stirring bar is used both as stirrer and as measurement tool. The torque on the bar was measured by the rheometer and later converted into a polymer concentration by calibration of the setup against polymer solutions of known concentrations ranging from 2.5×10^{-4} g g^{-1} to 1×10^{-3} g g^{-1}.

The vessel is initially filled with a volume of water of 6 mL. A mass of polymer powder of 6 mg ± 1 mg is introduced in the vessel at initial time. An initial step at a rotation speed of 50 rad s^{-1} for 5 seconds ensures the dispersion of the powder in the vessel. We visually check through the transparent vessel that powder is efficiently mixed in the bulk liquid at the end of this first step. In the subsequent measurement step, the rotation speed ω is set to its measurement value, in the range 1 to 70 rad s^{-1} and the torque increase is recorded over time, providing a measurement of the concentration increase over time during dissolution.

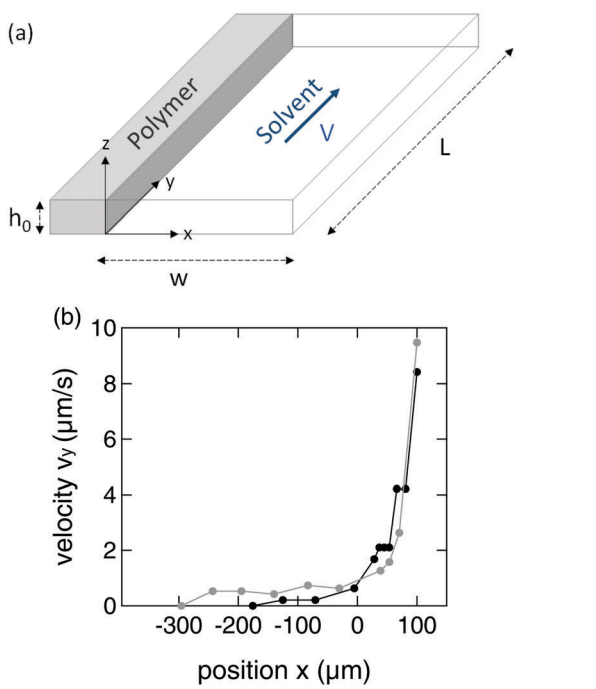

Fig. 4 (a) Schematic representation of the microfluidic channel: water flows in the y direction alongside the polymer layer in a thin channel of width w and height h_0, with a mean velocity V. The polymer/water interface location results from a competition between swelling and erosion by viscous shear. (b) Typical velocity profiles v_y in the gel for two different tracers (black/grey circles) as a function of the distance to the gel/solution interface x for a water velocity V = 0.2 m s^{-1}.

3 Dissolution kinetics in still solution

3.1 Swelling of a dry grain by a solvent: when a gel phase forms between dry polymer and solution

What is the mechanism limiting the kinetics of dissolution of polymers? In a preliminary experiment, we observe the dissolution kinetics of a series of polymer grains with typical size ranging between 10^{-5} m and 10^{-3} m. The grains are squeezed between two glass slides so that the swelling is quasi two-dimensional. A time series of images is shown in Fig. 2 for a grain of typical size 0.5 mm. Two interfaces can be identified: a solution/gel interface (dotted line in Fig. 2) and a gel/dry polymer interface (dashed line in Fig. 2). For a grain of size in the millimeter range, the dry core disappears within one minute, while it typically takes several tens of minutes for the gel to be dissolved. More precisely, the position of the two interfaces is monitored as a function of time by tracking a given value of light intensity at both interfaces on the recorded images. In Fig. 2(b), the gel thickness h and the position of the glass/gel interface relative to its initial position h_{glass} is plotted as a function of the square root of time and can be fit to a line with a prefactor $\sqrt{D}$: the dynamics of both interfaces is of diffusive type, and can be characterized by a diffusion coefficient D. In the case of Fig. 2, we find $D \sim 5 \times 10^{-9}$ m^2 s^{-1} and

$D_{glass} \sim 1 \times 10^{-9}$ m^2 s^{-1}: the diffusion coefficients at each interface are of the same order of magnitude, in agreement with the literature.

However, in the case of a glassy or semi-crystalline dry grain, one could expect a slow water penetration as compared with water fluxes through an entangled semi-dilute polymer solution, what is not observed experimentally. We suggest the imbibition of the dry polymer is faster than expected because either the dry polymer has a porous structure (for glassy polymers that are not annealed above glass transition temperature, this has been observed in the literature[23]) or swelling induces fractures in the dry core.[11] Whatever the effect at stake, we can nevertheless conclude that the kinetics of dissolution of the grain is not limited by the diffusion of water through the dry interface with the gel. Instead, the limiting step is the dilution of the gel.

3.2 What is the relaxation mechanism of the swollen gel network?

We now focus on the gel/solution interface. In the model derived by Brochard and De Gennes,[8] the slow dynamics for dissolution of long polymer chains is attributed to the reptation mechanism. Indeed, reptation time τ_{rep} strongly depends on molar mass as $\tau_{rep} \sim M_w^{\alpha}$ with $\alpha = 3$ in theoretical models and $\alpha = 3.4$ from experiments.[10] In the reptation model, the elastic stress built up within the gel upon swelling is relaxed by reptation of the entangled chains. As a consequence, a grain of semi-dilute polymer solution of initial radius h and initial concentration ϕ_0 should be dissolved within a characteristic time $t = h^2/D$ as long as diffusion is slower than the reptation mechanism. Consequently, the dissolution time t should have a minimum value, equal to the reptation time at initial concentration $\tau_{rep}(\phi_0)$: the minimum observable value for dissolution time is τ_{rep}, and a characteristic grain size l appears, which separates these two regimes: $l = \sqrt{D\tau_{rep}}$.

A direct comparison of our experimental data to this model can be drawn by analyzing the variations of the extent of the gel phase h as a function of the time t elapsed since the grain was put in contact with water. For $t/\tau_{rep} < 1$, the reduced time should tend to 1. For $t/\tau_{rep} > 1$, the gel extent should increase by diffusion of water in the gel with a diffusion coefficient D. Because τ_{rep} and D depend on the polymer concentration, the gel length h is reduced by the typical diffusive length $\sqrt{D\tau_{rep}}$ and time t is reduced by τ_{rep}. Within the approximation of polymer source and water reservoir of semi-infinite size, for $t/\tau_{rep} > 1$ the reduced time t/τ_{rep} should be a quadratic function of the reduced length $h/\sqrt{D\tau_{rep}}$. This prediction is plotted as t/τ_{rep} *versus* h/l as a dotted line in Fig. 5.

The swelling data for a series of grains of varied sizes were compared to the model. To do so, $\tau_{rep}(\phi)$ and D were first determined. On one hand, the polymer volume fraction ϕ_v was first calculated as the ratio between the thickness of the dry polymer that has entered in the gel phase h_{glass} and the current thickness h of the gel (Fig. 2b): $\phi_v = h_{glass}/h$. It was then converted into mass fraction ϕ using the polymer density ρ: $\phi = \dfrac{\rho}{(\rho - 1) + 1/\phi_v}$. Experimentally, the polymer concentration varies between 0.4 and 0.6 for the grain dissolution experiments, far larger than ϕ_E. The reptation time was then computed using eqn (1). On the other hand, the diffusion coefficient D was measured by fitting the data h *versus* $\sqrt{t}$ to a line, as in Fig. 2(b), with $\sqrt{D}$ as prefactor. The resulting reduced dissolution time t/τ_{rep} *versus* reduced length h/l corresponds to the full symbols in Fig. 5. In contrast to the theoretical prediction, we find that the reduced gel size has a diffusive dynamics as a function of the reduced time over 7 decades in time below τ_{rep}. Note that in Fig. 5 hollow symbols correspond to times above τ_{rep} from experiments that will be detailed in Section 3.3 and for which a diffusive behavior is also observed. Altogether, the diffusive swelling of the gel is observed over 10 decades in time, both above and below τ_{rep} what allows us to draw a strong conclusion: gel dilution is not limited by reptation, and reptation does not hinder the swelling of the polymer.

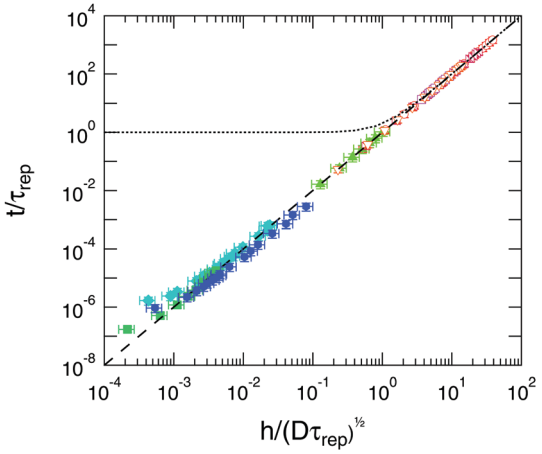

Fig. 5 Dotted line: prediction from Brochard *et al.*:[8] reduced dissolution time t/τ_{rep} as a function of reduced grain size h/l where l is the characteristic grain size $l = (D\tau_{rep})^{1/2}$ predicted to separate two dissolution regimes: for small grain sizes, the dissolution time is limited by the reptation time τ_{rep}; for grain sizes larger than l the dissolution time obeys a diffusive law in h^2 in the semi-infinite media approximation. Markers: our measurements of t/τ_{rep} as a function of h/l for two series of dissolution experiments in still water: full symbols: grain swelling at high concentration; hollow symbols: thin layer swelling measured by light scattering setup: data are recast in the frame of a semi-infinite source of polymer.

Indeed during swelling the stress in the swollen gel originates from two contributions, namely the stretching of the chains and their orientations. The first contribution deeply affects the osmotic pressure, while the second controls the deviatoric stress only. In addition, the first contribution relaxes with the contraction time of the chain in its tube – the respiration Rouse mode – and the second, which requires the chains to get rid of the entanglements, relaxes with the reptation time. Our results demonstrate that if there were a mechanism due to the chain dynamics hindering the swelling, this would only be due to the local stretching of chains, and not to their orientations. Obviously, adding solvent to the polymer results in a swelling of the transient gel, and consequently entangled polymer chains are stretched and an entropic stress arises. Simultaneously, the chains may contract in their Doi–Edwards' tube in order to

relax the chain extension. We develop a simple calculation to account for this process, which is developed in Appendix and yields a typical contraction time τ_{cont} which is the Rouse time of the chain in the tube, times a geometrical factor of 36. It increases as N^2 where N is the number of Kuhn segments of a single polymer while τ_{rep} is predicted to vary as N^3 and is measured to increase as $N^{3.3}$ experimentally.[10] Therefore τ_{cont} is $36N/N_e$ times smaller than τ_{rep}. The full expression for τ_{cont}/τ_{rep} is:

$$\frac{\tau_{cont}}{\tau_{rep}} = \frac{N_e}{36N} \quad (2)$$

Numerically, for the giant polyelectrolyte for which $N/N_e = 450$ and $\tau_{rep} = 2 \times 10^5$ s at $\phi = 0.1$ gives $\tau_{cont} \simeq 10$ s.

The contraction time is therefore much smaller than the experimental times, which is in agreement with our experimental observations. In other words, in the swollen entangled network, the relaxation of the stretched chains in their Edwards tubes is a fast process.

3.3 Dissolution kinetics at low polymer volume fractions

In order to probe the gel dissolution more accurately, we designed a new setup to probe much lower polymer volume fractions. The swelling kinetics of a polymer layer was measured by a quasi-one-dimension set-up described in the experimental section. In this experiment, the interface between the dry polymer and the gel cannot be observed but the concentration profile in the gel can be measured as a function of the distance z to the substrate. Fig. 6(a) presents a typical series of concentration profiles at various times for the giant polyelectrolyte. The concentration $\phi(z,t)$ obeys a diffusive equation:

$$\frac{\partial\phi(z,t)}{\partial t} = \frac{\partial}{\partial z}\left[D\frac{\partial\phi(z,t)}{\partial z}\right] \quad (3)$$

with initial condition $\phi(z < h_0, t = 0) = \phi_0$. Within the strong assumption that the diffusion coefficient of water D is independent of the polymer concentration, the diffusion equation yields:[24]

$$\phi(z,t) = \phi_0\left[\mathrm{erf}\left(\frac{h_0 - z}{2\sqrt{Dt}}\right) + \mathrm{erf}\left(\frac{h_0 + z}{2\sqrt{Dt}}\right)\right] \quad (4)$$

This theoretical result was used to fit the experimental profiles $\phi(z,t)$ with D as a fitting parameter. For the giant polyelectrolyte, we find $D = 2.5 \times 10^{-10}$ m^2 s^{-1} in the experimental concentration range (10^{-4} to 0.015 g g^{-1}). The measured value of the diffusion coefficient D can be compared to values from the literature measured by light scattering for polyelectrolytes:[17] for poly(*N*-benzyl-2-vinylpyridinium bromide) at concentrations ranging from 10^{-1} to 10^2 g L^{-1} in pure water, D is of order 10^{-10} m^2 s^{-1} and barely depends on the polyelectrolyte concentration in this range. Finally, the swelling of the gel is found to fully result from the diffusive flux of water inside the gel, in the narrow concentration range probed here, for which the hypothesis of constant D is reasonable, and in good agreement with the literature.

In order to compare the individual grain dissolution experiments of Section 3.2 to the present case where lower concentrations are obtained, the data were recast as if the semi-infinite media hypothesis used in Section 3.2 was holding. The height h of the gel at a given concentration $\phi_{gel} = 0.004$ g g^{-1} was measured as a function of time t. Because a diffusive behavior was found, the gel heights that would be obtained in a semi-infinite media experiment at equal times t were computed as $h = \sqrt{Dt}$ and added to the non-dimensional plot in Fig. 5 (hollow symbols) using the measured diffusion coefficient D and the calculated value for τ_{rep} from eqn (1). We find that they mostly correspond to times larger than τ_{rep}. Altogether, experimental reduced times t/τ_{rep} span over 10 decades for which the swelling of the polymer gel exhibits a diffusive kinetics shown as the dashed line. This further confirms that τ_{rep} is not special in any way, as in Section 3.2.

Finally, the swelling kinetics of the gel is found to be diffusive for any swelling time between 1 second and several days.

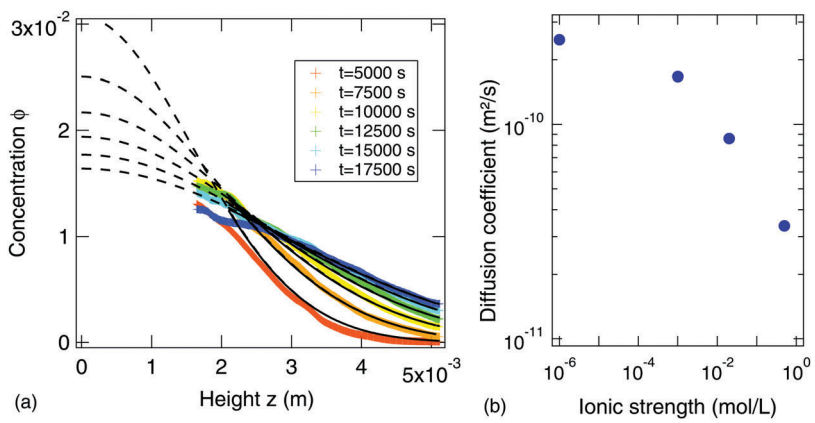

Fig. 6 (a) Lines: experimental polymer concentration profiles $\phi(z,t)$ as a function of the distance to the substrate z for the giant polyelectrolyte and for a series of times t since water was added ($h_0 = 50$ μm). Dotted lines: fitted concentration profiles according to the diffusive model (eqn (4)) with coefficient diffusion D as a parameter: $D = 2.5 \times 10^{-10}$ m^2 s^{-1} for deionized water. (b) Variation of diffusion coefficient D as a function of the ionic strength of the brine added.

3.4 What is the mechanism driving the solvent in the gel?

As explained above, the chain dynamics does not affect the gel swelling kinetics. The driving mechanism is thus the gradient in osmotic pressure between the dilute solution and the gel, which is balanced by the polymer network elasticity. With a polyelectrolyte, the osmotic pressure in the gel is set[25] by the ionic strength I, and decreases with I above a given threshold in salt concentration. This hypothesis was further verified by swelling layers of polyelectrolyte (h_0 = 50 μm) in aqueous solutions of salt (NaCl) with increased concentration C_{salt}. Concentration profiles were measured and were fitted to the diffusive model (eqn (4)) with a concentration-independent diffusion coefficient. Results are reported in Fig. 6(b) as a function of the ionic strength I where $I = C_{salt}$ for monovalent ions, and is estimated at 10^{-6} mol L^{-1} for pure water, thus accounting for the carbonate ions dissolved. We find that salt addition slows down the swelling kinetics, D decreases with I, showing how dilution of the gel is set by permeation of water from the dilute solution and driven in the polymer gel by the osmotic pressure gradient.

This result is in agreement with cooperative diffusion coefficients measured in the literature by light scattering experiments on polyelectrolyte solutions of varied salt concentration:[17] for poly(*N*-benzyl-2-vinylpyridinium bromide) at polymer concentration of 10^{-3} g g^{-1} and ionic strength ranging from 10^{-5} to 10^{-1} mol L^{-1} in pure water, D decreases from 10^{-10} to 10^{-11} m^2 s^{-1}. The diffusion coefficient is furthermore found to be independent of molar mass. At this stage, we therefore emphasize that the molar mass of the polymer does not modify the diffusion coefficient, because the relevant polymer length for water permeation (or diffusion) is the length between entanglements. In addition, the stretching of the polymer chains may control the swelling kinetics, but the contraction time in the tube τ_{cont}, which depends on the square of the molar mass, is much smaller than the experimental times and is therefore not limiting the dynamics within the range of experimental times. As a result, the whole swelling process of the network should not depend on the molar mass of the polymer. Yet, it is a well established result that the dissolution process of a polymer is molar mass dependent. We show in the next section that our experimental data corroborate that finding, and we provide, for the first time, a full explanation for that effect, which has often been erroneously attributed to a reptation driven relaxation of the swollen network.

3.5 How does the polymer molar mass affect dissolution?

In a second series of experiments, we used neutral polymers (PEO) with increased molar mass in order to assess the effect of the polymer chains length in the delaying of the gel dissolution in conditions where the driving osmotic pressure difference is unchanged. Swelling experiments in the 1D geometry (Section 2.4) were performed with layers of thickness h_0 = 50 μm of polyethylene oxides with varied molar mass. The resulting concentration profiles are shown in Fig. 7(a) for a molar mass of 1×10^6 g mol^{-1}. Interestingly, the behavior is very different from the giant polyelectrolyte one. Qualitatively, the area under the $\phi(z)$ curves roughly represents the total amount of polymer in the gel, in the observation window. Here, it is found that this quantity clearly decreases over time, what was not the case for the giant polyelectrolyte. This is attributed to a significant quantity of polymer having been dissolved in the dilute solution above the gel. The transfer from the gel into the dilute solution is accelerated by a spontaneous convective flux, that, although weak, is sufficient to efficiently disperse the polymer chains. Hence, concentration profiles from Fig. 7(a) could not be fitted to the solution of the diffusion equation with a constant diffusion coefficient (eqn (4)). We conclude that as the polymer simultaneously swells and dissolves in the solution, its concentration reaches the overlap concentration below which the dilute polymer chains are dispersed in the whole reservoir by natural convection.

An alternate representation of the data can be used at this stage: the height h of the gel at a given concentration is plotted as a function of time in Fig. 7(b). This concentration is chosen at $2\phi^*$ for every molar mass of PEO studied so that polymer chains are dispersed in solution. Indeed, at this concentration, the viscosity is low enough for the shear exerted by natural

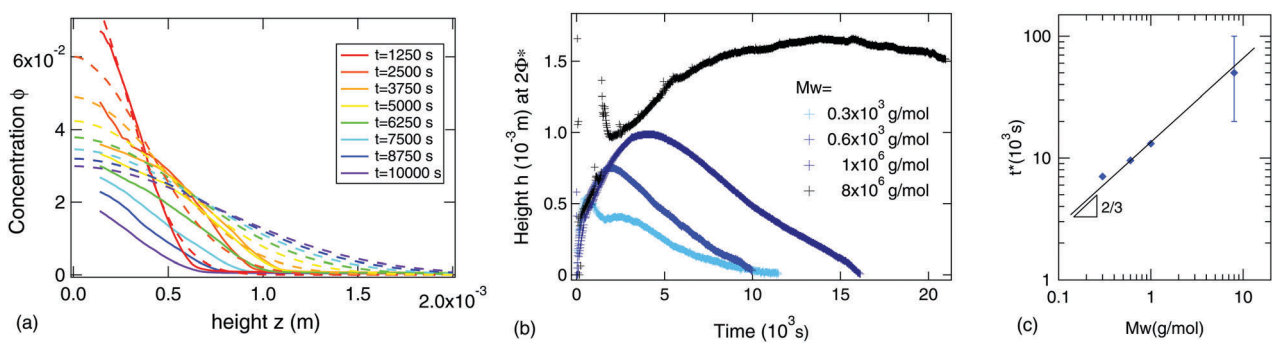

Fig. 7 (a) Lines: experimental concentration profiles $\phi(z,t)$ as a function of the distance z to the substrate for a polyethylene oxide PEO with molar mass $M_w = 10^6$ g mol^{-1}, and for a series of times since water was added. Dashed lines: calculated concentration profiles according to the diffusive model with a constant diffusion coefficient D (eqn (4)). This model clearly fails to fit the experimental curves: for $\phi < \phi_e$ the dilute polymers are dispersed in the reservoir. (b) Distance to the substrate as a function of time where the polymer concentration ϕ reaches $2\phi^*$ for a series of polyethylene oxides (PEO) with varied molar masses. A dissolution time t^* is defined as the time the height at concentration $2\phi^*$ has receded to the initial thickness of the dry layer h_0. (c) The dissolution time t^* as a function of the PEO molar mass can be fitted to a power law with exponent 2/3.

convection to be strong enough to disperse the polymer. The resulting $h(t)$ curves first increase, showing a first stage of swelling by diffusion, and after a certain time, the gel height recedes over time, which corresponds to a second stage where the polymer chains are dispersed faster into the dilute solution while water keeps diffusing into the gel. Obviously, the polymer is fully dissolved when concentrations smaller than the overlap concentration ϕ^* are reached. Hence, we have arbitrarily defined as characteristic dissolution time, the time t^* at which the iso-concentration curve corresponding to $\phi = 2\phi^*$ reaches the initial height of the dry layer h_0. So defined, the dissolution time t^* is found to increase with the molar mass of the polymer, as shown in Fig. 7(c). More precisely we find that t^* roughly varies with ${M_w}^{2/3}$. The exponent of the power law is much smaller than the one describing the variations of the reptation time with molar mass, which is in good agreement with previous findings.[1,7]

To conclude, we find that the swelling kinetics of high mass polymers is driven by the osmotic pressure gradient built-up across the gel/solution interface, leading to a diffusion of water through the polymer with a diffusion coefficient that strongly depends on polymer concentration, when concentration spans the whole range between dry and overlap concentration. The swelling yields internal stresses in the gel that, we suggest, are released by chain contraction in the Doi–Edwards tube within a short time, and not by reptation. By this mechanism, the gel swells down to the overlap concentration ϕ^*. Hence, the dissolution time is the time needed for the concentration at a typical distance h_0 to decrease down to ϕ^* and, as a result, it increases with the molar mass of the polymer. Below ϕ^* polymers are in a dilute regime and are dispersed in solution by natural thermal convection.

We will now turn to a study on the effect of mixing on the dissolution time for which convection is forced in the dilute phase. In particular, we investigate the effect of shear on the concentration at the gel/solution interface, which is equal to ϕ^* without shear.

4 Dissolution kinetics under stirring

It is well known that stirring efficiently decreases the dissolution time of polymer powders. In the following, we first focus on the effect of shear on the gel/solution interface and in particular on the gel concentration at which the gel is eroded. Second, we transpose our results to stirring experiments at a macroscopic scale where the polymer dissolution is monitored over time in a vessel equipped with a rotating bar.

4.1 What is the effect of shear at the gel interface?

We have designed a microfluidic setup to observe the polymer/water interface in a controlled geometry and under imposed shear, so as to observe simultaneously the polymer swelling and its erosion by the solvent flow. This study was performed with the polyelectrolyte. It is schematically depicted in Fig. 4. The position x of the gel/water interface evolves over time: it is set by a balance between polymer swelling, that tends to displace the interface towards larger x-values, and the erosion process, that oppositely displaces the interface towards smaller x-values. The latter mechanism results from the shear stress applied in the y-direction.

The stress applied to the gel interface is the viscous stress built-up in water σ. The latter can be estimated using an order of magnitude of the velocity gradient in the x-direction. As mentioned in Section 4.1, the water velocity decreases from V to a vanishing value at the interface over the typical distance set by the channel height h_0, and finally $\sigma = \eta_0 \frac{V}{h_0}$ where η_0 is the water viscosity. At the interface, the tangential stress is constant and thus equal to σ. Besides, in the polymer layer, tracers are used to monitor the gel deformations: the velocity v_y along the y direction is measured as a function of the distance x to the interface (Fig. 4b) and the strain rate $\dot{\gamma}$ is estimated as the ratio of the velocity change δv_y in the polymer over the typical distance h_0.

The stress σ and shear rate $\dot{\gamma}$ can therefore be obtained at the interface for a series of shear rates in the water flow. As calibration curves, rheology characterization of polymer solutions with varied polymer concentration were used to extract the polymer concentration at the eroded interface ϕ_{er} from the given $(\sigma, \dot{\gamma})$ data. The rheology curves $(\sigma, \dot{\gamma})$ are plotted in Fig. 8(a) for different polymer mass fractions: the gel is eroded at a given value of the shear stress σ so this series of rheological curves is converted in Fig. 8(b) into a graph where the shear rate is the y-axis, polymer mass fraction is the x-axis and the shear stress σ is a parameter. In this way, we clearly find that the position of the gel/solution interface is given by the polymer mass fraction ϕ_{er} for which, under a given stress, the gel yields, with the shear rate rapidly changing from a low value in the gel ($\dot{\gamma} < 10^{-2}$ s^{-1}) up to a large value in the solution ($\dot{\gamma} \gg 10^{2}$ s^{-1}) within a very narrow range in concentration between points A and B (in Fig. 8(a–c), points A and B correspond to each other). Thus we define the erosion concentration ϕ_{er} as the polymer mass fraction taken in point A. From this, we conclude that the measurement of the rheology of polymer solutions of varied mass fractions can be directly used to measure the erosion concentration ϕ_{er} as a function of the shear applied to the gel interface.

By choosing different values of the shear stress applied by the flowing solution to the gel interface, a series of shear rate *versus* polymer concentration was obtained and is plotted in Fig. 9(a) with shear stress as a parameter for each curve. The erosion concentration is measured at the downward step of the shear rate on each curve, and is plotted in Fig. 9(b) as a function of the shear rate in the solvent. We emphasize that the erosion concentration under given shear conditions is entirely set by the rheology of the polymer solutions. Obviously, the polymer concentration at which the gel is eroded increases as the shear rate increases. In the following, we derive a relationship between erosion concentration and shear rate in the water. The shear stress σ is constant at any point of the polymer solution, from the dilute polymer solution to the gel phase. It can be equivalently calculated at the interface (point A: $\sigma_A = \eta\dot{\gamma}_A$) or far away from the eroded interface, in the dilute solution for which

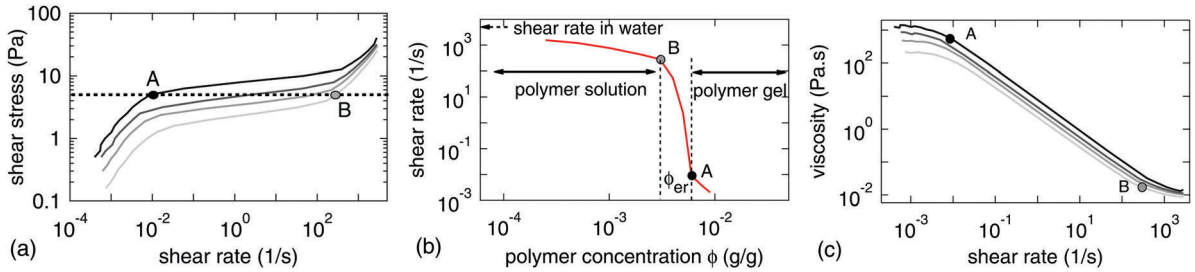

Fig. 8 Rheological measurements performed with aqueous solutions of the polyelectrolyte. (a) Shear stress *versus* shear rate for varied polymer concentrations ϕ (bottom to top: $\phi = 3.10^{-3}$, 4.10^{-3}, 5.10^{-3}, 6.10^{-3} g g^{-1}). Dashed line corresponds to a shear stress $\sigma = 5$ Pa. Between points A and B, the shear rate increases by 4 orders of magnitude for a given shear stress. (b) Shear rate *versus* polymer mass fraction at a given shear stress $\sigma = 5$ Pa. Within a narrow range of polymer fraction, the shear rate drops by 4 orders of magnitude: the value of the polymer mass fraction at point A is taken as the erosion concentration. (c) Viscosity *versus* shear rate in rheology experiments: point A, where erosion takes place, is given by the end of the Newtonian plateau for large enough shear stresses.

the viscosity is close to the water viscosity η_0 ($\sigma = \eta_0\dot{\gamma}_w$). The polymer mass fraction at the solution/gel interface corresponds to the end of the Newtonian plateau in viscosity *versus* shear rate curve (Fig. 8c), so that at point A, the shear rate is related to the mass fraction by: $\dot{\gamma}_A = {\phi_{er}}^{-3/2}/\tau_0$ (from eqn (1)). Moreover, the Newtonian plateau viscosity of entangled polymer solutions is expected to vary with mass fraction such that $\eta \sim \eta_0\phi^3$ – and so it does in our case (see Section 2.1); therefore, the shear stress at the eroded interface can be written as: $\sigma_A = \eta\dot{\gamma}_A \sim {\phi_{er}}^3{\phi_{er}}^{-3/2}/\tau_0 \sim \eta_0/\tau_0{\phi_{er}}^{3/2}$. On the other hand, far from the eroded interface, the shear stress also writes $\sigma = \eta_0\dot{\gamma}_w$ and equals σ_A. The erosion concentration can finally be written as:

$$\phi_{er} = (\tau_0\dot{\gamma}_w)^{2/3} \qquad (5)$$

where τ_0 was measure in Section 2.1. We have found a very good agreement between experimental data and eqn (5), as shown in Fig. 8(b). The same power law is found with and without salt addition, but with a different prefactor, showing a decrease of τ_0 with increasing ionic strength. That decrease is however rather small with respect to the corresponding variation of ionic strength, reflecting the weak sensitivity of the rheological behaviour to the salt content. In the following, we will show that the prediction for the erosion concentration allows for a deep understanding of the dissolution process under stirring.

4.2 Dissolution in macroscopic stirring conditions

In a second step, the erosion process was studied at a macroscopic scale by using a stirring experiment in which the stress applied to stir at a constant speed is measured as polymer is added to a given volume of water. Polymer concentration as a function of time can thus be inferred (see Section 2.6 for details).

The polymer used was the polyelectrolyte. A typical curve is shown in Fig. 10(a) where concentration is plotted as a function of elapsed time in the measurement setup. Concentration is found to increase towards a plateau value at $\phi_\infty = 1 \times 10^{-3} \pm 0.02$ g g^{-1} showing that full dissolution of the polymer mass was achieved. We define the dissolution time $t_{1/2}$ as the time to reach half the final concentration ϕ_∞. A series of experiments at varied rotation speed ω was performed in order to measure the variations of the dissolution time $t_{1/2}$ with effective shear rate.

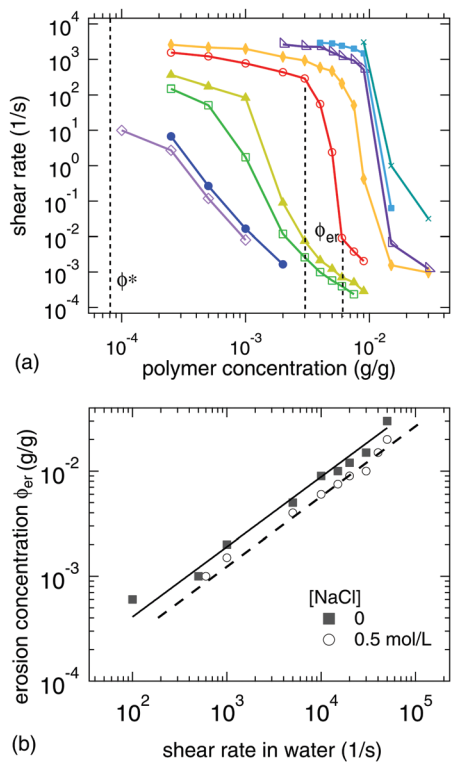

Fig. 9 (a) Shear rate $\dot{\gamma}$ in the polymer solution as a function of the polymer concentration ϕ from flow rheology measurements. Each curve corresponds to a given shear stress σ: from bottom to top curve: $\sigma = 0.05$, 0.1, 0.5, 1, 5, 10, 20, 30, 50 Pa. (b) Erosion concentration ϕ_{er}, defined as the polymer mass fraction at the gel/solution interface, as a function of the shear rate in the eroding aqueous solutions. Deionized water and NaCl solution at 0.5 mol L^{-1} were used. Lines: fit to a power law with exponent 2/3.

Results are plotted in Fig. 10(b). The dissolution time $t_{1/2}$ *versus* ω data can be fitted to a power-law curve with exponent -1.2.

In addition, we have performed the same experiments but in brine. We have observed that the rheological behaviour is in practice only slightly affected by the presence of salt as explained above. However, we observe in Fig. 10(c) that an increase of ionic strength significantly increases the time for dissolution. As the rheological behavior of the polymer solutions is barely

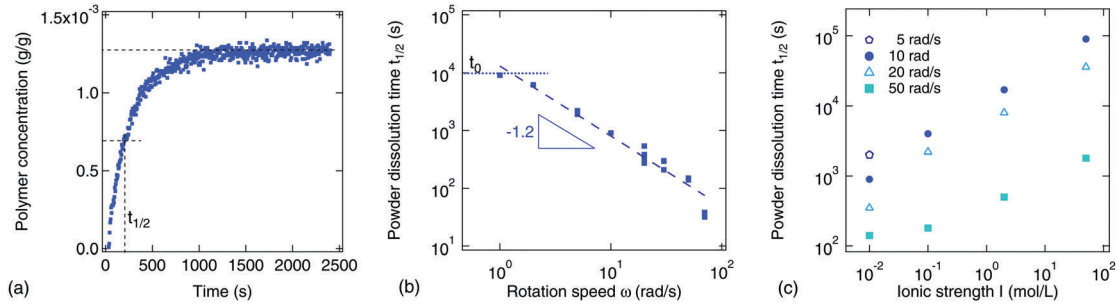

Fig. 10 (a) Polymer concentration increase over time during the dissolution of powdered dry polymer in a vessel with controlled stirring. Rotation speed ω = 50 rad s^{-1}. The dissolution time $t_{1/2}$ is defined as the time to reach half the final concentration. (b) Dissolution time $t_{1/2}$ *versus* rotation speed ω in pure water and (c) *versus* ionic strength of NaCl solution in the vessel for different rotation speeds.

modified by a change in ionic strength, this can originate only in the variation of the diffusion coefficient with ionic strength, see Fig. 6(b).

In the following we derive a model to bridge these observations at a macroscopic scale to the results obtained at the gel/solution interface in Sections 3 and 4.1. We will derive an estimate of the dissolution time under stirring. First, we expect that the dissolution time cannot be larger than the limit value measured at zero shear. In Section 3, the limit value, we denote as t_0, was found to be set by the time needed for water to diffuse in the grain until the polymer concentration in the grain decreases down to the dispersion concentration. For the polyelectrolyte, we take the entanglement concentration ϕ_E. For an initial grain radius R_i, the final swollen grain radius relevant for dissolution is thus given by $\phi_E \sim \frac{R_i^3}{R_f^3}$ if density differences are neglected. The limit value for the dissolution time can therefore be estimated as $t_0 = \frac{R_f^2}{D} = \frac{R_i^2}{D\phi_E^{2/3}}$. With $D = 10^{-10}$ m^2 s^{-1}, dry grain size R_i = 50 μm and $\phi_E = 8 \times 10^{-5}$ g g^{-1} we find $t_0 = 10^4$ s. This upper limit is added to Fig. 10(b) as a dotted line and agrees well with the data for which $t_{1/2}$ tends to t_0 at vanishing rotation speed ω.

An estimate of the effect of stirring on the rate of dissolution can now be provided. The discussion above establishes that the erosion concentration of the polymer depends on the applied shear stress. However, we need to estimate the quantity of polymer that is detached per unit of time, which constitutes a convection/diffusion coupled problem,[26] and it is well known that the flux of matter is related to the thickness of the erosion layer. This thickness itself is determined by the competition between the diffusion – that increases the thickness by swelling – and the convection – that decreases the thickness of the layer, by replacing the swollen polymer by fresh solution. This thickness is roughly given by:

$$\xi \sim \sqrt{D\tau} \tag{6}$$

where τ is the time for convection to renew the solution. This time τ is given by the displacement of the fresh solution divided by its velocity at the surface of the erosion layer:

$$\tau \sim R(\dot{\gamma}\xi)^{-1} \tag{7}$$

where R is the particle radius. Combining the two previous equations gives for ξ:

$$\xi \sim (DR\dot{\gamma}^{-1})^{1/3} \tag{8}$$

The expression for the thickness of the boundary layer is very similar to the one for the dissolution of a moving sphere with a velocity U if U is replaced by $\dot{\gamma}/R$.[26] The erosion rate can be inferred from that last equation. Indeed the flux of polymer per surface unit is $j \sim \phi_{er}D/\xi$. Hence, an estimate for the dissolution time is:

$$t_{diss} \sim R\phi_0/j = \frac{\phi_0}{\phi_{er}} R^{4/3} D^{-2/3} \dot{\gamma}^{-1/3} \tag{9}$$

Hence, the dissolution rate not only depends on the shear rate but also on the mutual diffusion coefficient D. The full dependence on the shear rate is obtained by using eqn (5) that describes the variation of the erosion volume fraction ϕ_{er} with shear rate $\dot{\gamma}$. Finally, the scaling law for the dissolution time writes, with a prefactor of the order of 1:

$$t_{diss} \sim R^{4/3} D^{-2/3} \dot{\gamma}^{-1} \tau_0^{-2/3} \tag{10}$$

Comparison of the model eqn (10) for $t_{diss}(\dot{\gamma})$ to the experimental data $t_{1/2}(\omega)$ can be made. First, as shown in Fig. 10, the dissolution time decreases with increasing rotation speed (or, equivalently, shear rate) following a power law with an exponent −1.2. This exponent is close to the expected −1, and the discrepancy between theory and experiment can be attributed to the fact that the flow in the cell is not laminar, and vorticity may develop at large rotation speeds. However, the trend of variation with shear rate is well captured. Second, the effect of the diffusion coefficient is unambiguous. As previously mentioned, we have found that a variation in ionic strength significantly modifies the value of the diffusion coefficient, whereas the prefactor τ_0 of the erosion volume fraction remains of the same order of magnitude. We find that an increase in ionic strength induces a decrease in the diffusion coefficient and thus an increase in the dissolution time, as predicted by the model eqn (10). Finally, a numerical estimate of t_{diss} can be obtained from eqn (10) using the following typical values: grain diameter R = 50 μm, time $\tau_0 = 2 \times 10^{-6}$ s from eqn (5), diffusion coefficient $D = 2 \times 10^{-10}$ m^2 s^{-1} from Fig. 6(b), a shear rate $\dot{\gamma} \sim 4\omega$ (where 4 stands for the ratio of the vessel diameter to

the stir bar length), and a rotation speed $\omega = 10$ rad s^{-1}. We find $t_{diss} = 5 \times 10^3$ s whereas we measure $t_{1/2} = 10^3$ s. Given approximations we made, the agreement between theoretical t_{diss} and experimental $t_{1/2}$ is satisfying and our model accounts semi-quantitatively for the dissolution time of polymer grains in a stirred vessel of solvent.

5 Conclusions

The dissolution of polymer powders can be quantitatively described using a few simple arguments:

(1) In agreement with previous findings, the glass/melt transition upon solvent uptake is not a limiting process for dissolution. The limiting process is instead the dilution of the transient gel phase constituted by the swollen polymer in the entangled semi-dilute regime.

(2) In contrast to previous analyses, the reptation process does not hinder swelling of the network, and the chains relax by contraction in their tube, which is generally a fast process compared to the overall dissolution process.

(3) Without stirring, the dissolution occurs when the volume fraction reaches the overlap concentration. As a consequence, the dissolution is strongly dependent on the molar mass of the polymer.

(4) Under large enough stirring, the polymer gel is eroded and shear occurs within a very thin layer, due to its non-linear rheology. The volume fraction in this erosion layer depends on the shear rate. As a consequence, the erosion process is analogous to a dissolution/convection problem.

Polymer powder dissolution in a solvent is generically described using three different steps:[27] first, polymer grains sprinkled at the solvent surface must be wetted by the solvent, what can be very slow.[28] Second, grains must be dispersed in the bulk solvent so as to obtain individual grains surrounded by solvent.[29] The third step, namely the swelling and erosion of individual grains, has been semi-quantitatively described in the present paper, both in still water and under stirring, using simple scaling laws. Altogether, we anticipate that the mechanisms at stake during dissolution of powders of polymers elucidated in this study will be transposed to practical situations given that simple rheological characterizations and grain sizes only are needed to get orders of magnitude of the dissolution times.

6 Appendix: model for swelling of entangled chains by contraction in Doi–Edwards tube

This Appendix details the theoretical derivation of the typical time at stake when a network of entangled polymers swells in a good solvent. Solutions are assumed to be in the semi-dilute regime and polymers are described within the real chain framework, by the Kuhn's model. Entanglements are described with Doi–Edwards' tube model. Here, we describe a mechanism where a swollen polymer network, initially at equilibrium, swells upon solvent addition. The polymer network consequently extends and chains stretch between entanglements, which corresponds to an increase of the curvilinear length of the chain Edwards' tubes. Simultaneously, chains relax inside their tube by contraction so that the length relaxes to the equilibrium size $L_{eq}(\phi)$ set by the new solvent volume fraction $1 - \phi$.

In the framework used, N is the chain monomer number, b is the length of a Kuhn segment, ϕ is the polymer volume fraction of the semi-dilute solution. For a real chain in good solvent in equilibrium, the equilibrium curvilinear length of a chain is $L_{eq} = \frac{N\xi}{g}$, where $g(\phi)$ is the number of monomers per correlation blob and $\xi(\phi)$ is the correlation blob size. Using classical relations between those quantities,[10] one finds easily that $L_{eq} \sim Nb\phi^{\frac{1-\nu}{3\nu-1}} \sim Nb\phi^{1/2}$ taking 3/5 for the exponent ν, the exact value of ν being 0.588. Thus the curvilinear chain length – in blobs – increases with polymer volume fraction. To estimate the relaxation time after an increment of volume fraction, we split the chain response in two stages.

First, in response to a variation of polymer volume fraction from ϕ to $\phi - \delta\phi$, the chain stretches in its tube to an out-of-equilibrium length $L = L_{eq} + \delta L$ which is equal to both the tube and the chain length. During this first step, the volume is changed from V to $V + \delta V$ and the chain elongation is assumed to homothetically follow the macroscopic deformation. As a consequence, the ratio L^3/V, or equivalently $L^3\phi$ remain constant. This writes: ${L_{eq}}^3\phi = (L_{eq} + \delta L)^3(\phi - \delta\phi)$ yielding $\delta L = L_{eq}\frac{\delta\phi}{3\phi}$. In the meantime, the equilibrium length varies with volume fraction according to: $\delta L_{eq} = L_{eq}\frac{-\delta\phi}{2\phi}$. Altogether, for an infinitesimal variation of the volume fraction $\delta\phi$ during the time δt, the chain is driven to an out-of-equilibrium length stretch equals to $\delta(L - L_{eq}) = L_{eq}\frac{5\delta\phi}{6\phi}$.

In a second step, we let the chain relax to its new equilibrium length. The chain relaxation occurs by contraction of the chain inside the tube due to the stretching entropy S calculated from the probability that a primitive chain has a contour length L.[21] This yields: $S = -k\left(\frac{3(L - L_{eq})^2}{2Nb^2}\right)$ where k is the Boltzmann constant. The entropy gain by contraction is associated with a driving free energy density per unit chain and unit time $E_d = -\frac{\partial(TS)}{\partial t}$. This yields:

$$E_d = \frac{3kT}{Nb^2}(L - L_{eq})\frac{\partial(L - L_{eq})}{\partial t} \qquad (11)$$

During contraction, every monomer moves with a velocity v, and thus experiences a viscous friction force $\vec{f}_v = \zeta\vec{v}$ where ζ is the friction coefficient per monomer. This viscous force translates into a dissipation of energy that balances the driving free energy E_d given by eqn (11). We will next derive equations to model the dissipative energy E_v. As the swelling deformation of the network is isotropic, the monomer velocity v depends

linearly on the curvilinear position along the tube sL with $0 \leq s \leq 1$. By symmetry, $v(s = 0.5) = 0$ and $v(s) = -\left(s - \frac{1}{2}\right)2u$ where u is the velocity of the end of the chain given by: $2u = \frac{\partial(L - L_{eq})}{\partial t}$. The energy density dissipated by viscous friction per unit chain and unit time E_v writes: $E_v = \int_0^1 N\vec{f_v} \cdot \vec{v}\mathrm{d}s$. Altogether, E_v writes:

$$E_v = \frac{1}{12}N\zeta\left(\frac{\partial(L - L_{eq})}{\partial t}\right)^2 \quad (12)$$

The driving energy density E_d is balanced by the dissipative energy density E_d through $E_d = E_v$, leading to:

$$\frac{\partial(L - L_{eq})}{\partial t} = \frac{36kT}{N^2b^2\zeta}(L - L_{eq}) \quad (13)$$

Here we assume that the chain relaxation has a unique relaxation time τ_{cont}, and as a result:

$$\tau_{cont} = \frac{\zeta N^2 b^2}{36kT} = \frac{\tau_R}{36} \quad (14)$$

where τ_R is the Rouse time of the respiration mode. So the contraction time is similar to the Rouse longest relaxation time up to a geometrical factor. The contraction is thus faster by many order of magnitude than the reptation time. The reptation time is given by[10] $\tau_{rep} = \tau_R N/N_e$ where N_e is the number of monomers per entanglements and the ratio between the two relaxation times is given by

$$\tau_{cont} = \frac{N_e}{36N}\tau_{rep} \quad (15)$$

References

1 B. Narasimhan and N. A. Peppas, *Polym. Anal.*, 1997, **128**, 157–207.
2 B. A. Miller-Chou and J. L. Koenig, *Prog. Polym. Sci.*, 2003, **28**, 1223–1270.
3 B. Narasimhan, J. E. M. Snaar, R. W. Bowtell, S. Morgan, C. D. Melia and N. A. Peppas, *Macromolecules*, 1999, **32**, 704–710.
4 A. Parker, F. Vigouroux and W. F. Reed, *AIChE J.*, 2000, **46**, 1290–1299.
5 D. G. Bucknall, J. S. Higgins and S. A. Butler, *J. Polym. Sci., Part B: Polym. Phys.*, 2004, **42**, 3267–3281.
6 S. Abrahmsen-Alami, A. Korner, I. Nilsson and A. Larsson, *Int. J. Pharm.*, 2007, **342**, 105–114.
7 S. Ugur, A. K. Dinc and Y. Kislak, *J. Polym. Res.*, 2012, **19**, 9943.
8 F. Brochard-Wyart and P.-G. De Gennes, *PhysicoChem. Hydrodyn.*, 1983, **4**, 313–322.
9 Q. Wang, P. R. Ellis and S. B. Ross-Murphy, *Carbohydr. Polym.*, 2008, **74**, 519–526.
10 M. Rubinstein and R. Colby, *Polymer Physics*, Oxford University Press, 2003.
11 A. Turner, E. Gurnee and W. Lloyd, *J. Polym. Sci., Part C: Polym. Symp.*, 1966, **12**, 249–261.
12 W. Ogieglo, H. Wormeester, M. Wessling and N. E. Benes, *Macromol. Chem. Phys.*, 2013, **214**, 2480–2488.
13 W. Ogieglo, H. Wormeester, M. Wessling and N. E. Benes, *Polymer*, 2013, **54**, 341–348.
14 H. E. Hermes, C. E. Sitta, B. Schillinger, H. Loewen and S. U. Egelhaaf, *Phys. Chem. Chem. Phys.*, 2015, **17**, 15781–15787.
15 T. M. Hyde and L. F. Gladden, *Polymer*, 1998, **39**, 811–819.
16 M. Engelsberg and W. Barros, *Phys. Rev. E: Stat., Nonlinear, Soft Matter Phys.*, 2013, **88**, 062602.
17 S. Forster, M. Schmidt and M. Antonietti, *Polymer*, 1990, **31**, 781–792.
18 R. Colby, *Rheol. Acta*, 2010, **49**, 425–442.
19 G. Marrucci, *J. Non-Newtonian Fluid Mech.*, 1996, **62**, 279–289.
20 G. Iannirubertо and G. Marrucci, *J. Rheol.*, 2014, **58**, 89–102.
21 M. Doi and S. Edwards, *The Theory of Polymer Dynamics*, Clarendon Press, 2009.
22 K. Devanand and J. Selser, *Macromolecules*, 1991, **24**, 5943–5947.
23 C. M. Hansen and L. Just, *Ind. Eng. Chem. Res.*, 2001, **40**, 21–25.
24 J. Crank, *The Mathematics of Diffusion*, Clarendon Press, 1975.
25 A. Dobrynin, R. Colby and M. Rubinstein, *Macromolecules*, 1995, **28**, 1859–1871.
26 V. Levich, *Physicochemical Hydrodynamics*, Prentice Hall, Englewood Cliffs, NJ, 1962.
27 L. Forny, A. Marabi and S. Palzer, *Powder Technol.*, 2011, **206**, 72–78.
28 F. Lequeux, L. Talini, E. Verneuil, G. Delannoy and P. Valois, *Eur. Phys. J. E: Soft Matter Biol. Phys.*, 2016, **39**, 12.
29 J. Dupas, L. Forny and M. Ramaioli, *J. Colloid Interface Sci.*, 2015, **448**, 51–56.